DETECTION OF SUBTLE RIDGELINES FROM LASER SCANNING DATA

Amit Baruch, Sagi Filin

Dept. of Transportation and Geo-Information Eng., Technion – Israel Institute of Technology, Haifa 32000, Israel -
(amit, filin)tx.technion.ac.il

Commission III, WG 3

KEY WORDS: airborne laser scanning, feature extraction, breaklines, curvature, active contours, geomorphology

ABSTRACT:

Airborne laser scanning technology is primarily perceived as a means for gathering detailed three-dimensional information about the surface and objects on it. It is therefore not surprising that the majority of the laser related research has focused on the detection of the terrain within the point cloud and on distinct surficial objects like building roofs and tree canopies. Nonetheless, the dense 3D data contains information about linear entities, some of which are of subtle form. While some of the efforts have been made into extracting linear elements from laser scanning data, the attention was mostly turned to dominant elements that are very clear and distinct. We present in this paper a model for the detection of linear features of various sizes and magnitudes laser data. Our focus is on the detection of subtle linear elements. We apply the model to detect and extract paleo shorelines that have the form of small ridges. Such fossil shorelines are clear markers of receding lakes and record the annual high and low stands. Results show that ridges of ~20 cm height can be identified and separated from the surrounding features in data.

1. INTRODUCTION

Airborne laser scanning has been used for mapping applications for more than a decade seeing the lion's share of research focusing on the extraction of the terrain (see e.g., Sithole and Vosselman, 2004), of salient objects like buildings (e.g., Vosselman and Dijkman, 2001, Brenner, 2005) or of roads and trees (Clode et al., 2004, Vosselman, 2003, Yu et al., 2004). As a result, features extraction models were mostly associated with the detection of surface segments usually of planar ones (Lee and Schenk, 2001; Vosselman, 2001; Filin, 2002; Hofmann, 2004). In contrast, the detection of linear elements has received little attention so far or was only considered as a byproduct of surface extraction procedures, e.g., roof ridgelines that resulted from the intersection of neighboring planes (e.g., Vosselman and Dijkman, 2001).

Focusing on the extraction of linear features, Brügelmann (2000) presents an edge-extraction based approach seeking breaklines in dense laser datasets. The focus is on salient features, aiming to add linear constraints to digital terrain models. The model is based on finding lines of extreme curvature values in the data, and its application is demonstrated on a fairly dense dataset (7 points/m^2) showing a relatively smooth object (a dike), with a set of relatively distinct lines. Briese (2004, 2006) presents a semi-automated approach which is based on following lines of maximum curvature. Contrasting Brügelmann (2000), the detection of points with high curvature values is implemented in a similar fashion to the extraction of the roof ridges. Local planes are fitted in both sides of the seed points (according to its direction) and if the angular difference between them is strong enough, the line is extended. The process terminates when the curvature value drops below a preset threshold value. Brzank et al. (2005) detects breaklines by first applying a step edge-detection operator (Canny) to approximately locate lines where strong enough responses occur. The extracted lines are then used for fitting tangential hyperbolic surfaces. As the authors

point, the predefined surface shape around the line is assumed, which may not fit in all cases. Rutzinger et al., (2006), outlines an object-based extraction framework and demonstrate it on the extraction of moraines. A preset definition of the phenomena distinctiveness dictates the search window and curvature related parameters. Features are extracted by skelatonization of high curvature regions. In Lantz et al., 2003, a set of predefined filters, which are based on surface inclination and orientation, are used for identifying different types of object features like roads and ditches. This detection is based on seeking angular difference according to the set of filters and is valid to well-defined and sharp transitions.

Nonetheless, lines showing in laser data can be a result of much subtler transitions, ones whose saliency will rather be associated with their elongated form than the actual edge (step or crease) response. We study in this paper the detection of subtle linear features in airborne laser scanning data. The lines of interest here are paleo shorelines, which are linear entities formed as a result of lakes retreat. We propose an autonomous model for their detection and characterization, and demonstrate the ability of LiDAR driven models to detect land-features of minute size and on large-scale.

The reminder of the paper is structured as follows; we begin with a short description of the shoreline formation process and demonstrate their realization along the coastal plains. The presentation of the proposed methodology for LiDAR based shorelines detection follows. As we show, several phases are involved in the detection, but it is their agglomeration that leads to the ability to detect shorelines in various forms. Following the presentation of the model, results and analysis that demonstrates the application of the algorithm conclude the presentation.
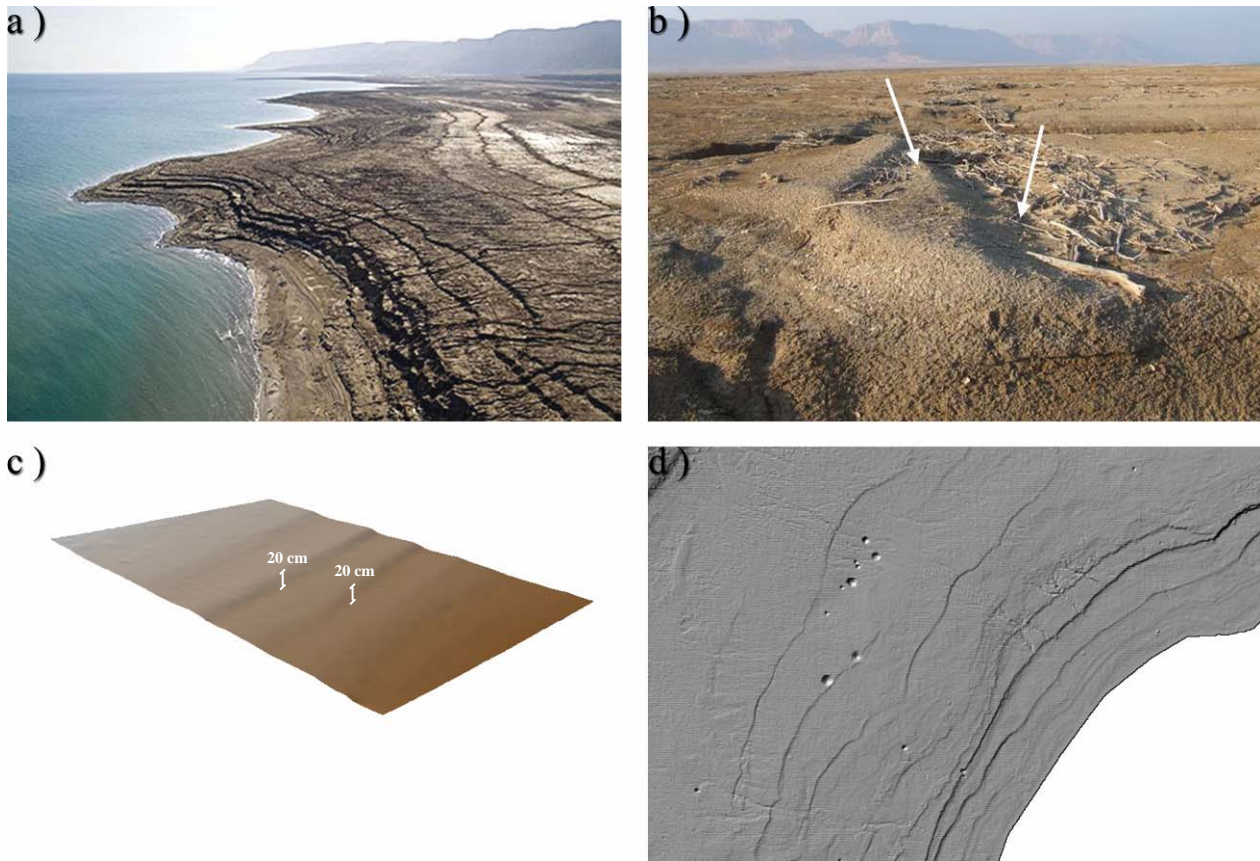
Figure 1. Shorelines along receding lakes, a) a side looking aerial view showing shorelines in different phases, b) shoreline whose actual realization as a line is being mainly marked by drifted wood, c) the realization of shorelines as show in laser scanning data, d) different realization of the shorelines in the LiDAR data showing their diversity and variability.

2. FORMATION AND REALIZATION OF SHORELINES

Formation of shoreline sequences can generally be ascribed to receding lake levels, usually as a result of water diversion, or extensive water use (see e.g., Street-Perrott and Harrison, 1985; Abelson et al., 2006). As the lake retreat, a set of deserted shorelines, appearing as topographically elevated beach-ridges, are left behind on the costal plain. The formation of the beach ridges is related to the wave impact during spring storms. The precise location of each shoreline marks the uppermost elevation that the lake level reached during the winter and spring before the gradual slow retreat during the dry season. In cases where the drop of water-level is rapid, the created shorelines from every year are preserved. Normally, the wave action in the next winter does not reach the previous beach ridge after the level has dropped during the summer, and so one shoreline will consist of two linear features, one for each season. Shorelines therefore serve as annual markers that record past water levels during periods of decrease and are useful in reconstructing episodes of lake retreat. Through time the clear steps become subjected to changes, and are modified by gully formation, incision of pre-existing stream channels, and runoff erosion. We also note that in rare episodes during unusually rainy winters the level rise and the wave actions erode previous shorelines. In addition to erasing preceding shorelines, the erosion caused by the rising water creates a conspicuous large step, which is preserved by the subsequent drop of the water. The morphology of modern steps is readily correlated to recorded precipitation.

Figure 1 illustrates the nature of the shorelines. In Figure 1a, a side looking view of well-preserved sequence of shorelines, with steps of ~30 cm high, are clearly seen. In Figure 1b, a solitary shoreline located in an exposed coastal plain is seen. Here the main manifestation of the step is in the very narrow line mostly defined by drifted wood. Figures 1c and 1d show the realization of shorelines in the LiDAR data. The two sets differ by the underlying topography, but in both cases the steps are ~20 cm high. The notable fact is that the actual edge is not well defined and was eroded over time, almost to blend with the underlying topography. We note that even though those lines are expected to form equal height contours, tracing their actual elevation shows that they do not preserve a constant height. This has to do with erosion coupled with the effect of the surface topography.

3. DETECTION MODEL

Geometrically, shoreline sequences can be described as composed of coupled linear features representing a local extrema in the surface curvature (see Figure 1). The higher linear features relate to the seasonally-high water stand, and be characterized by locally minimal curvature values. The lower lineaments, representing the seasonal low-stand, are featured conversely by locally maximal curvature values. Shoreline sequences therefore alternate signs from negative (winter) to positive (summer), where within each zone (positive or negative) their actual location will be along the local extremum value. Nonetheless, because of surface erosion and noise, the extracted features will only form a set of fragmented lines. An agglomeration of the fragments into a complete, descriptive

feature should then follow. Our proposed model is therefore built on a framework that first detects regions within which shorelines are expected to lie, then finds their outlines, and finally connects compatible fragmented shorelines into a single entity. In the following, each stage is discussed in detail.

3.1 Detection of seed shorelines region

Shoreline points will be described as forming a local extrema in the surface curvature. They can be quantified by the Hessian form, **H**

$$\mathbf{H} = \begin{pmatrix} \dfrac{\partial^2 Z}{\partial x^2} & \dfrac{\partial^2 Z}{\partial x \partial y} \\ \dfrac{\partial^2 Z}{\partial x \partial y} & \dfrac{\partial^2 Z}{\partial y^2} \end{pmatrix} \tag{1}$$

with Z the heights as derived from the LiDAR data. For a stationary point to be a valley or a ridge point, **H** must be semi-positive or semi-negative definite respectively, and so, having one eigenvalue that equals to zero (more realistically, close to), while the other is either positive for summer or negative for winter ridges. We compute **H** numerically via

$$\partial^2 Z / \partial x^2 = \left(Z_{y_0, x_0+d} - 2 \cdot Z_{y_0, x_0} + Z_{y_0, x_0-d} \right) / (d)^2$$
$$\partial^2 Z / \partial y^2 = \left(Z_{y_0+d, x_0} - 2 \cdot Z_{y_0, x_0} + Z_{y_0-d, x_0} \right) / (d)^2 \tag{2}$$
$$\partial^2 Z / \partial xy = \left(-Z_{y_0-d, x_0-d} + Z_{y_0-d, x_0+d} + Z_{y_0+d, x_0-d} - Z_{y_0+d, x_0+d} \right) / (2d)^2$$

with d the window size. While polynomial derived estimations (e.g., Besl, 1988; Mitášová and Hofierka, 1993) can also be considered an option, the numerical estimation we apply is both computationally efficient and can easily adapt to characterizing the variety of sizes, shapes, forms and directions that shorelines wear. In the following section we describe its adaptation into a multi-scale analysis.
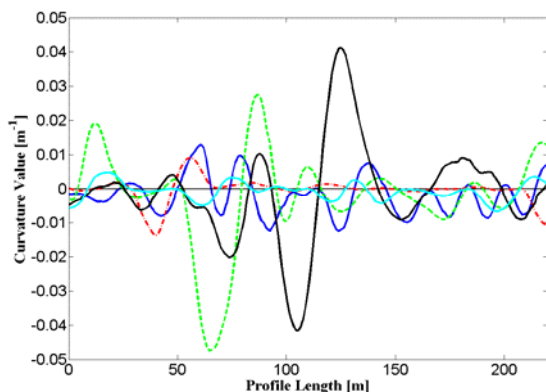
Figure 1. Curvature along profiles extracted across the coastal plains in different sites, showing different magnitudes, other than the two strong peaks, all ridges are smaller than 1 m and on average are ~20 cm high.

3.1.1   Multi-scale parameter analysis

The common practice for the detection will be applying a fixed kernel size and searching for sufficiently strong responses (in Brügelmann, 2000 low pass smoothing by a Gaussian filter is applied to attenuate noise effect). As Figure 2 shows, in the current case it is almost impossible to set a predefined threshold value that will manage capturing "strong" responses relating to the locally maximal curvature. Additionally, smoothing the data to attenuate noise effect might blur the shorelines and eliminate them. Because of the variety of forms and surface texture characteristics, responses may have different magnitudes. Therefore, the surface curvature and the eigenvalues computation are performed in multi-scale manner, in different levels from fine to coarse, searching for a "significant" response. To assess the responses, the retrieved parameters are studied in terms of the limit of detection.

Limit of detection – A ridge, or a seasonally high water stand shoreline related point, requires one of the eigenvalues derived from **H** to be positive and the second to be equal to zero, namely $\lambda_1 < 0$ and $\lambda_2 = 0$. Similarly, a valley, or the seasonally low water stand shoreline related point, requires $\lambda_1 > 0$ and $\lambda_2 = 0$. Deriving an upper and lower bound responses level, ε_1 and ε_2, such that $|\lambda_1| > \varepsilon_1$ and $|\lambda_2| \le \varepsilon_2$, can either be approached by learning from examples, or be estimated theoretically by deriving accuracy estimates for λ_1 and λ_2 as a function of the elevation accuracy. Since our objective is finding the minute detectable shorelines, we analyze the LiDAR driven bounds. The accuracy of λ_1 and λ_2 is controlled by the second-order partial derivatives (assuming that second-order mixed derivatives equals to zero in ridge and valley points) accuracy as derived from Eq. (2). Following the propagation of the elevation accuracy onto these parameters and onto the eigenvalues we obtain

$$m_{\lambda_{1,2}} = \pm \frac{\sqrt{6}}{d^2} m_Z \tag{3}$$

with $m_{\lambda_{1,2}}$ the accuracy estimate of the eigenvalue, and m_z the laser elevation accuracy. Two hypothesis tests are formed, one for λ_1, with H_0: $\lambda_1 \le 0$ as the null hypothesis and H_1: $\lambda_1 > 0$ as the alternative, and the another for λ_2 with H_0: $\lambda_2 = 0$ as the null hypothesis and H_1: $\lambda_2 \ne 0$ as the alternative. For a given confidence level α, the two hypotheses provide bounds for shorelines detection, with

$$\left| \frac{\lambda_1 - 0}{m_\lambda} \right| > z_{1-\alpha} \quad \Rightarrow \quad |\lambda_1| > z_{1-\alpha} \cdot m_\lambda =$$
$$z_{1-\alpha} \cdot \frac{\sqrt{6}}{d^2} m_Z = 1.645 \cdot \frac{\sqrt{6}}{d^2} m_Z \quad (\text{for } \alpha = 5\%) \tag{4}$$

$$\left| \frac{\lambda_2 - 0}{m_\lambda} \right| \le z_{1-\frac{\alpha}{2}} \quad \Rightarrow \quad |\lambda_2| \le z_{1-\frac{\alpha}{2}} \cdot m_\lambda =$$
$$z_{1-\frac{\alpha}{2}} \cdot \frac{\sqrt{6}}{d^2} m_Z = 1.96 \cdot \frac{\sqrt{6}}{d^2} m_Z \quad (\text{for } \alpha = 5\%) \tag{5}$$

with z the normalized Gaussian distribution. Equations (3), (4) and (5) show that $m_{\lambda_{1,2}}$ is scale dependent and with the increase of d (scale decrease), λ will be estimated more accurately. Therefore, instead of setting a unique threshold for the entire scene, each point will be examined via its own Z-test, for a scale which can accommodate the first significant response. The result of this procedure will be regions with significant positive and negative responses.

In Figure 3 we demonstrate the seed regions in which responses that are strong enough to trigger detection were found. The different coloring reflects the levels in which a response was recorded. As can be seen even within the seed region of a single shoreline, there are detections in different levels of resolution. In this case they can be attributed to changes in the underlying surface topography and their weathering.

3.2 Detection of the shoreline curve

The detection of the actual shoreline locations is triggered by the seed region that can be regarded as topographic bound for the exact location of the curve. The curve should follow the extremum of the terrain curvature (principal curvature), and preferably be smooth. The exact location is identified, in most cases, by a change in the curvature gradient value. Both shape and boundary constraints are accommodated by casting the problem as energy minimization in which the shoreline curve is modeled as an active contour whose shape is guide by internal, spline, and external, path, forces (Kass et al., 1988). Representing the position of the contour as $x(s)$, with s as the arc-length parameter, its energy functional can be written as

$$E_c = \int_0^1 E_c\left(x(s)\right)ds = \int_0^1 E_{\text{int}}\left(x(s)\right) + E_{ext}\left(x(s)\right)ds \qquad (6)$$

with E_c, the contour energy, E_{int}, the internal spline energy, and E_{ext}, the external energy arriving from the terrain (by means of the LiDAR data). The internal spline energy is composed of a

first- and second- order terms aiming controlling the length of the curve arcs, and its smoothness respectively

$$E_{\text{int}} = \left(\alpha\left|x'(s)\right|^2 + \beta\left|x''(s)\right|^2\right)\Big/2 \qquad (7)$$

with α, controlling the first-order, and β the second-order terms (α and β can also be set as functions of s but they are usually, as here, set as constants). The optimal curve should minimize Eq.(6), and must satisfy Euler equation

$$\alpha x''(s) - \beta x''''(s) - \nabla E_{ext} = 0 \qquad (8)$$

with the internal force, $\alpha x''(s) - \beta x''''(s)$, discouraging the stretching and bending, and the external potential force, ∇E_{ext}, forcing the curve to converge towards the shoreline path. The external energy function, E_{ext}, is derived from the laser data, and given $K(x, y)$, the terrain curvature, $f(x, y)$, which is the change in curvature will be used for the external energy with

$$\nabla E_{ext} = -\nabla K(x, y) = -f(x, y) \qquad (9)$$

Since the internal energy is influenced by the spline setup, it is the external energy that drives the contour to its actual location. We initialize the curve from the medial axis of the seed region which theoretically will be close enough to the final desired location (we note that looking for local exterma will be a more aware choice, however this is being taken care of the active contour).
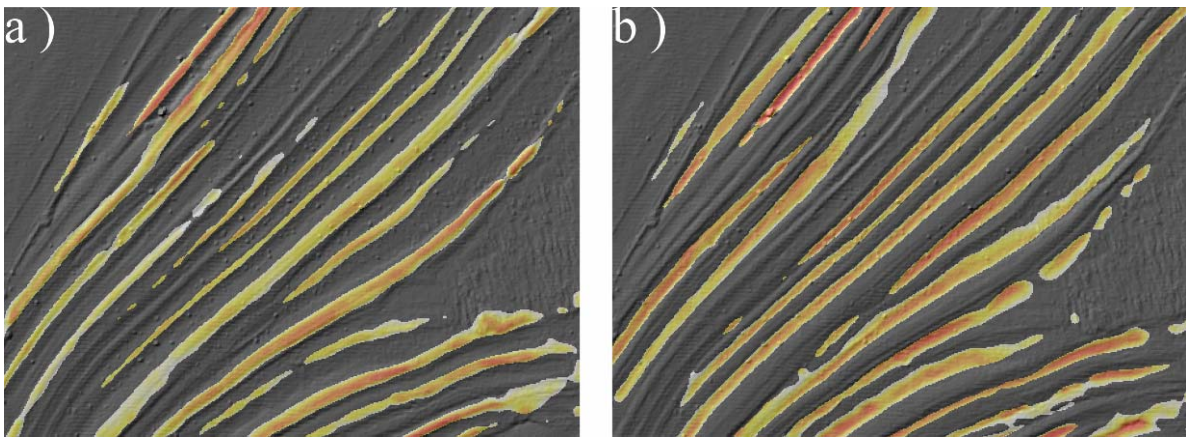
Figure 2. The detected seed regions for, a) the wet season, b) the dry season, the different colouring within the regions reflect the resolution levels in which a response was recorded (hot colours – small scales). Notice that even within single shoreline seed region there are detections in different levels of resolution.

3.3 Connecting fragmented features

Erosion processes, surface roughness, measurements noise and formation of small channels across the ridgeline, lead to disconnections in the extracted shorelines, both in those relating to the dry and wet seasons. The curvature signal will therefore be too weak to pass the statistical test needed to trigger a response. It is therefore likely that a given ridgeline will be broken into several, individual, segments. As the objective of the model is to extract the ridgeline in an as complete form as possible, those undetected gaps should be bridged. The proposed approach for connecting fragmented shorelines is divided into two complementary stages; the first selects the candidate line pairs to be connected, the second finds the optimal path in terms of energy minimization and consistency of the overall sequence. This path tracking focuses on accumulating weak signals into a meaningful linear feature that will connect the two strong lines in both its ends. For generality the two stages are driven without making use of prior knowledge. For shorelines, such knowledge can relate to their height, and so, height difference criterion will lead to a considerable decrease of the search space (disqualifying pairs whose the height difference exceed a given threshold).

3.3.1 Limiting the matching candidates

Without any prior knowledge, each of the detected lines will be treated as a fragment with all the other lines sharing similar sign considered an appropriate match. We maintain a line continuity criterion assuming that lineamental features should preserve their local orientation. Based on the orientation criterion a set of candidate shorelines to connect are considered for each probed shoreline fragment.

3.3.2 Finding an optimal path

Linking the two candidate lines can be cast as a path finding problem. As noted, surface curvature signals in disconnected areas are weak but still exist. We therefore apply a tracking strategy that is based on finding a path that minimizes the energy involved in traversing this area. Energy will be measured in terms of curvature values by looking at paths between two pairs of end points and searching for the shortest path in term of curvature values, namely

$$d\left(\overline{p}\right) = \sum d\left(i,j\right)_{(i,j)\in\overline{p}} = \min\left(\sum d\left(i,j\right)_{(i,j)\in p}\right) \qquad (10)$$

with p, a candidate path between the two end points, $\overline{p}$ the shortest path, and $d(i,j)$ the weight between two consecutive points. For wet season lines the terrain curvature values will be negative, and therefore weights will be assigned as $d(i,j) = K(j)$. For the dry season shorelines, the curvature values will be positive. Therefore, to achieve minimum energy we flip the signs for the weights, namely $d(i,j) = -K(j)$.

Ridgelines cannot intersect among themselves and the upper part of the ridge cannot intersect with its lower part (which we term its negative reflection). Therefore, following the path finding between the edges, a logical consistency test of the linking paths is performed. Our implementation simply removes links that intersect other lines, but we note that by grading all analyzed links for each end point, it is possible to find an optimal combination that maintains the ridgeline topology. An alternative is finding the *k*-shortest paths (see Yen, 1971;

Shibuya, 1995) and eliminate intersections (particularly between the ridgeline and its negative reflection).
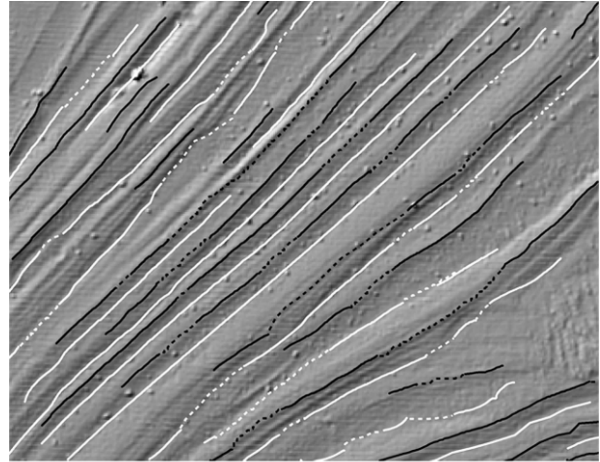
Figure 3. Detection of sequence of shorelines, with black wet season shorelines, and white dry season related

4. RESULTS AND DISSCUSION

We demonstrate the application on three regions featuring different characterizations, acquired along the Dead Sea coastal plain. Since the mid-1960s, increasing diversion of water from its northern Dead Sea drainage basin started a continuous process of artificial drop in the lake level, which was accelerated since the 1970s, reaching an average rate of 1 my^{-1} in the last 10 years. At present the lake level extends 28 m lower than the early 20th century high stand. The resulting environmental deterioration along the coastal plains was featured in soil erosion and incision of channels which were forming with the exposure of the coastal plains, and the formation of surface discontinuities, e.g., due to shoreline exposure (see Figures).

In Figure 4, a sequence of shorelines can be seen, with ridge height of ~20 cm. The seed regions from which the detection was initialized are shown in Figure 3. As Figure 3 illustrates, the detection of the wet season shorelines has stronger responses compared to the dry season ones. This difference in responses can be attributed to effect of surface erosion, which in smoothing the beach ridge makes the lower part of the ridge less distinct. As can be seen in Figure 4, the lines generally follow the ridges (and their negative reflections) and that the gap bridging has managed keeping track with the ridge line. In the lower part of the shore (upper left corner) the detection has limited level of success. This can be attributed to the relatively steeper slopes of the overall topography there (resulting in a denser set of shorelines). The curvature analysis there had therefore difficulties overcoming the strong carrying surface signal.

In Figure 5 we demonstrate the detection of shorelines where channels that were formed along the edge incise them. In Figure 5a the detection of ridgelines and their negative reflections is shown. It is not surprising to notice that in addition to the shorelines the channels ridges were extracted as well. To separate the two different ridges we categorize them by the general orientation, which results in two distinct clusters (see Figure 5b). In Figure 5c we show the ridge (positive and

negative) related points belonging to the north-west south-east lines following the connection of the fragmented lines. It can be seen that the minimal path was the one crossing the channels. It is optimal within the potential set of path that could link the points.
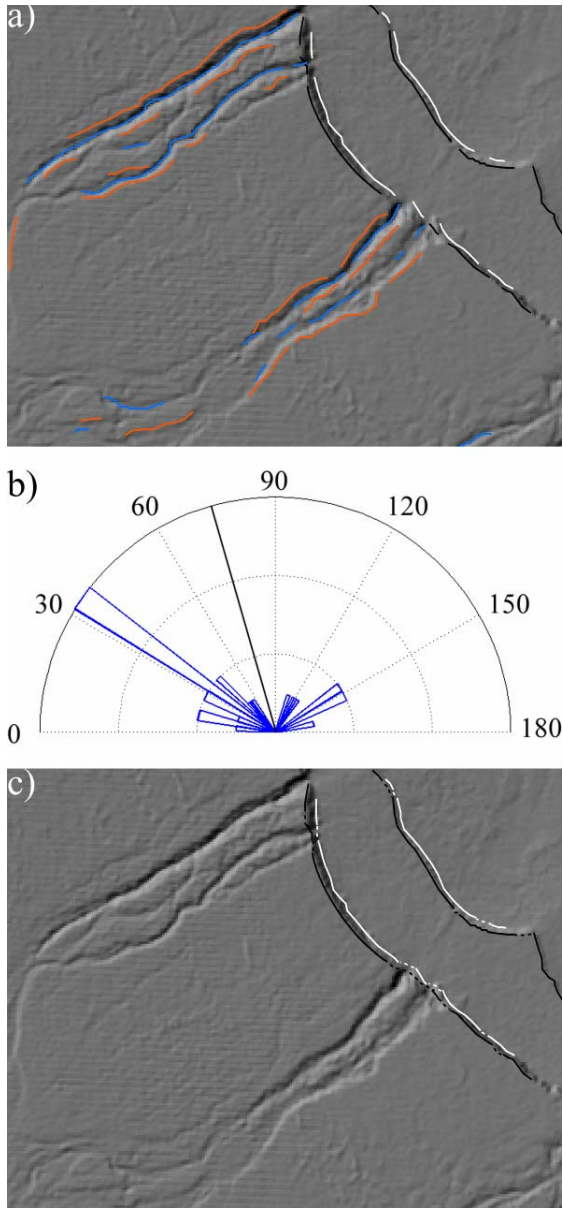
Figure 4. Detection of shorelines where the ridges are dissected by channels, a) the result of the ridgeline extraction, b) a polar histogram showing the orientations, c) the shorelines related segments (wet – black and dry – white)and the with the bridged gaps (dashed).

Finally, Figure 6 shows the extraction of the shorelines that from the data shown in Figure 1d. The area there is relatively flat at the upper part with a modest slope developing as it approaches the lake. In the flat part, the shorelines are hardly noticeable after undergoing erosion. The shorelines also differ from one another in the curvature magnitude, again alluding to the need for a multi-resolution based analysis. The results show that while being subtle in appearance, the detection model has managed identifying them, and where the response was too weak and no candidate counterpart of connection existed, the

line did not develop further. Overall the results show that the ridgeline detection model has manage identifying subtle lines of ~20 cm height within large regions, these results illustrate the great potential of LiDAR derived applications in extracting fine features geomorphic or others.
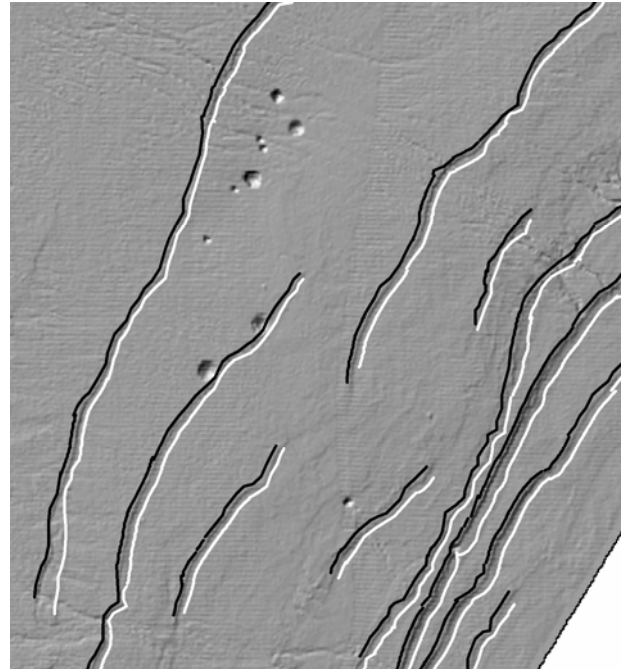
Figure 5. Detection of shorelines for the dataset in Figure 1d, with black wet season shorelines, and white dry season related.

5. CONCLUSIONS

We presented in this paper a model for the extraction of ridgelines from airborne laser scanning data. Differing from edge based approaches the proposed model seek areas which are homogenous in their curvature sign and with values significant enough to overcome background noise. The use of multi-scale approach allows detecting different ridge realizations. This removes the need to define what strong edge should be and allows focusing on subtle ones. The use of active contour to converge into the actual ridgeline allows integrating both external, surface constraints, with internal, line related ones, thereby controlling local noise effect. Casting the bridging as a path finding problem allows modeling the connection in terms of energy minimization problem. The results show how the proposed approach has managed identifying subtle ridgelines.

ACKNWOLEDGEMENT

REFERENCES

Abelson M., Y. Yechieli, O. Crouvi, G. Baer, D. Wachs, A. Bein and V. Shtivelman (2006). "Evolution of the Dead Sea sinkholes." Geological Society of America Special Paper 401: 241-253.

Besl P. J. (1988). "Surfaces in Range Image Understanding." Springer -Verlag, New York.

Brenner C. (2005). "Building reconstruction from images and laser scanning." International Journal of Applied Earth Observation and Geoinformation 6(3-4): 187-198.

Brzank A., P. Lohmann and C. Heipke (2005). "Automated extraction of pair wise structure lines using airborne laserscanner data in coastal areas." International Archives of Photogrammetry, Remote Sensing and Spatial Information Sciences 36(3/W19).

Clode S., P. Kootsookos and F. Rottensteiner (2004). "The Automatic Extraction of Roads from Lidar Data." International Archives of Photogrammetry, Remote Sensing and Spatial Information Sciences 35(B3).

Filin S. (2002). "Surface clustering from airborne laser scanning data." International Archives of Photogrammetry and Remote Sensing 34(3A): 117-124.

Hofmann A. D. (2004). "Analysis of tin-structure parameter spaces in airborne laser scanner data for 3-d building model generation." International archives of photogrammetry and remote sensing 34(B3): 302-307.

Kass M., A. Witkin and D. Terzopoulos (1988). "Snakes: Active Contour Models." International Journal of Computer Vision: 321-331.

Lantz F., E. Jungert and M. Sjövall (2003). "Determination of Terrain Features in a Terrain Model from Laser Radar Data." Proceedings of the ISPRS working group III/3 workshop, Dresden, Germany, 8-10 October 2003

Lee I. and T. Schenk (2001). "3D perceptual organization of laser altimetry data." International archives of photogrammetry and remote sensing 34(3/W4): 57-65.

Mitášová H. and J. Hofierka (1993). "Interpolation by Regularized Spline with Tension II: Application to terrain modeling and surface geometry analysis. ." Mathematical Geology 25(657-669).

Rutzinger M., B. Höfle, N. Pfeifer, T. Geist and J. Stötter (2006). "Object based analysis of airborne laser scanning data for natural hazard purposes using open source components." International Archives of Photogrammetry, Remote Sensing and Spatial Information Sciences 36(4/C42).

Vosselman G. (2001). "3D building model reconstruction from point clouds and ground plans." International archives of photogrammetry and remote sensing 34(3/W4): 37-43.

Vosselman G. (2003). "3D Reconstruction of Roads and Trees for City Modeling." International Archives of Photogrammetry, Remote Sensing and Spatial Information Sciences 34(3/W13).

Vosselman G. and S. Dijkman (2001). "3D Building Model Reconstruction From Point Clouds and Ground Plans." International Archives of Photogrammetry and Remote Sensing 34(3/W4).

Yu X., J. Hyyppä, H. Kaartinen and M. Maltamo (2004). "Automatic detection of harvested trees and determination of forest growth using airborne laser scanning." Remote Sensing of Environment 90(4): 415-423.